REVISTA INVESTIGACION OPERACIONAL
https://doi.org/10.5281/zenodo.23302382 **VOL. 48, NO.1, 81-94, 2027**

1D HYDRAULIC DESIGN AND CROSS-VERIFICATION WITH STEADY CFD OF AN ARCHIMEDES SCREW TURBINE: DIMENSIONAL AND DISCREPANCY AUDIT

Luis Navarrete López[1], Jefferson Porras Reyes, Damián Albán Andrade
Universidad Técnica de Cotopaxi, Ecuador.

ABSTRACT

Archimedes screw turbines are gravitational, low-head machines whose preliminary sizing is usually done with a one-dimensional hydraulic model and then examined with computational fluid dynamics. This paper reports that sequence for a bench-scale prototype and, above all, audits what the comparison between the two models can and cannot establish. A 1D hydraulic design supplies the operating point; a steady, single-phase, incompressible CFD model of one helical segment in a rotating reference frame under the frozen-rotor approximation supplies the three-dimensional fields. Two audits are then applied. The first is dimensional: the published operating point does not close the hydraulic energy balance, and the geometric scale documented in the study's own figures — a computational domain 0.242 m high and about 0.437 m long, with a velocity field bounded by 12.79 m s^{-1} — excludes the cubic-meter reading of the discharge and bounds the hydraulic power available from the documented geometry at approximately 6.2 W, far below either interpretation of the reported power, so that neither the absolute power nor the efficiency can be verified: the net head is undocumented and no shaft torque is reported. The second audit is cell-wise. The published comparison table contains seven non-zero-reference entries, six numerically within 15 %; however, the provenance of the two pressure entries is inconsistent with the displayed CFD pressure field, so only the five velocity comparisons can presently be interpreted physically. Of those, four fall within 15 % and the tangential velocity at the screw inlet differs by 59.04 %, with an origin that cannot be established from the available record. The 15 % figure is the claim being audited, not a general acceptance criterion. No grid-convergence study, residual history or near-wall resolution could be recovered, so the CFD results are one numerical realization rather than mesh-independent predictions, and the agreement reported here is cross-verification between two models of the same designer, not experimental validation. Beyond this turbine, the transferable contribution is the four-gate protocol itself (Section 2.4): an ordered, weight-free sequence that determines which claims about model fidelity remain available after each check, and when escalating to a more expensive computation or to the laboratory is warranted.

KEYWORDS: Archimedes screw turbine; low-head hydropower; computational fluid dynamics; model verification; dimensional analysis.
MSC: 76D05, 65Z05, 76M12.

RESUMEN

Las turbinas de tornillo de Arquímedes son máquinas gravitacionales de bajo salto cuyo dimensionamiento preliminar suele hacerse con un modelo hidráulico unidimensional y examinarse después con dinámica de fluidos computacional. Este trabajo reporta esa secuencia para un prototipo de banco y, sobre todo, audita qué puede y qué no puede establecer la comparación entre ambos modelos. El diseño hidráulico 1D aporta el punto de operación; un modelo CFD estacionario, monofásico e incompresible de un segmento helicoidal en marco de referencia rotatorio, bajo la aproximación de rotor congelado, aporta los campos tridimensionales. Se aplican después dos auditorías. La primera es dimensional: el punto de operación publicado no cierra el balance de energía hidráulica, y la escala geométrica documentada en las propias figuras del estudio —un dominio computacional de 0,242 m de altura y unos 0,437 m de longitud, con un campo de velocidad acotado por 12,79 m s^{-1}— excluye la lectura en metros cúbicos del caudal y acota en aproximadamente 6,2 W la potencia hidráulica compatible con la geometría documentada, muy por debajo de cualquiera de las interpretaciones de la potencia reportada, de modo que ni la potencia absoluta ni el rendimiento pueden verificarse: el salto neto no está documentado y no se reporta par en el eje. La segunda auditoría es celda a celda. La tabla de comparación publicada contiene siete entradas con referencia no nula, seis de ellas numéricamente dentro del 15 %; sin embargo, la procedencia de las dos entradas de presión es incompatible con el campo de presión que muestra la propia figura CFD, de manera que solo las cinco comparaciones de velocidad pueden interpretarse físicamente. De ellas, cuatro quedan dentro del 15 % y la velocidad tangencial en la entrada del tornillo difiere en 59,04 %, con un origen que el registro disponible no permite establecer. El 15 % es la afirmación auditada, no un criterio general de aceptación. No se pudo recuperar estudio de convergencia de malla, historial de residuos ni resolución de pared, de modo que los resultados CFD son una realización numérica y no predicciones independientes de la malla, y la concordancia reportada es verificación cruzada entre dos modelos del mismo diseñador, no validación experimental. Más allá de esta turbina, la contribución transferible es el propio protocolo de cuatro compuertas (Sección 2.4): una secuencia ordenada y sin pesos que determina qué afirmaciones sobre la fidelidad del modelo quedan disponibles tras cada comprobación, y cuándo se justifica escalar hacia un cálculo más costoso o hacia el laboratorio.

PALABRAS CLAVE: turbina de tornillo de Arquímedes; hidroelectricidad de bajo salto; dinámica de fluidos computacional; verificación de modelos; análisis dimensional.

[1] Corresponding author: luis.navarrete7284@utc.edu.ec.

1. INTRODUCTION

The Archimedes screw turbine is a gravitational, low-head machine. Water enters at the upper end, successively fills the cavities formed between the helix and the channel, descends under the action of gravity and, in doing so, turns the rotor: the available power is fixed by the product of the flow rate and the head difference between the upstream and downstream water levels, not by the kinetic energy of a free stream. This distinction is not terminological. Horizontal-axis hydrokinetic machines submerged in a current [2, 20, 21] extract energy from an unconfined flow and their efficiency scales with the cube of the current velocity; the machine studied here works confined in a channel and its efficiency scales with the available head. In what follows, the term gravitational is used for the device studied, and hydrokinetic is reserved for the literature that actually deals with free-stream machines.

Interest in these machines for small-scale distributed generation is well documented, both in terms of performance measured at real installations [11, 12] and in the assessment of their potential in micro-hydropower [10]. Simplified hydraulic screw theory [17] and performance models with variable fill level [15] provide the usual one-dimensional framework for preliminary sizing, and published design methodologies oriented toward clean generation exist [1, 19]. The effect of the number of blades on flow and performance has been studied both numerically and experimentally [7, 9], and there are experimental characterizations of hydrodynamic behaviour against flow rate and load [22].

The design of one of these turbines is usually organized in two stages. First, a one-dimensional hydraulic model fixes the operating point — flow rate, head, rotational speed, inclination and basic screw dimensions — from correlations and empirical coefficients [19]. Then a three-dimensional computational fluid dynamics (CFD) simulation allows the internal field to be examined: pressure distribution, recirculation and velocity patterns along the helical channel [6, 18, 21]. The comparison between the two stages is frequently presented as the design verification.

That presentation conceals a methodological problem that this work takes as its object. Comparing a 1D model with a CFD model built from the outputs of that same 1D model is not validation: it is cross-verification between two representations of the same design hypothesis, made by the same team, with the same boundary conditions. It can detect internal inconsistencies, and that has value, but it cannot certify the model against physical reality. Certifying it requires measuring torque, flow rate, head and efficiency on the prototype, and that contrast exists in the literature [22] but is not carried out here.

This paper's contribution is, therefore, narrower and more verifiable than that of a conventional design study, and it is stated unambiguously. First, a dimensional consistency audit of the published operating point, which contrasts flow rate, power, head and velocity scale against the geometry documented in the study's own figures. Second, a disaggregated, cell-by-cell comparison between the 1D design and the CFD model, instead of a single summary figure. Third, an explicit statement of which part of the computational record exists and which does not, and what can consequently be claimed. And fourth, a gated verification protocol that orders these checks as a decision sequence on model fidelity, which is the transferable part of the work.

No design optimization is presented: no search procedure over the geometric parameter space has been carried out, and the text does not use the term in its mathematical sense. Nor is experimental validation presented.

2. METHODOLOGY

2.1 One-dimensional hydraulic design

The starting point is a one-dimensional hydraulic model implemented in in-house code, built on standardized geometric relations, empirical performance coefficients and friction-loss curves of the kind collected in the screw-sizing literature [19]. The set of parameters governing that sizing — pitch, number of blades, inner and outer radii, inclination and length — and its effect on theoretical performance have been systematically analysed [3, 5], and detailed descriptions exist of the procedure applied to small-scale prototypes like the one studied here [8, 16]. The model's input data are the net head, the volumetric flow rate, the angular velocity, the inclination angle and the channel dimensions; the design variables the program allows to be varied are the number of blades, the length-to-diameter

ratio and the estimated hydraulic efficiency. Its outputs are the local hydraulic properties along the channel, the screw's geometric parameters and the estimated useful power.

The hydraulic power available in a gravitational machine is obtained from the head and the flow rate, per Eq. (1):

$$P_{\mathrm{h}} = \rho g Q H \tag{1}$$

where ρ is the density of water, g the acceleration of gravity, Q the volumetric flow rate and H the net head between the upstream and downstream water levels. Shaft power and hydraulic efficiency are related to it through Eq. (2):

$$P_{\mathrm{s}} = T\omega, \quad \eta = \frac{P_{\mathrm{s}}}{P_{\mathrm{h}}} \tag{2}$$

with T the shaft torque and ω the angular velocity. These two relations are what allow the consistency of the operating point to be audited in Section 3.1: any triplet (flow rate, power, head) that does not satisfy them is internally inconsistent, regardless of the quality of the hydraulic model that produced it.

2.2 Operating principle and prototype scale

Figure 1 schematizes the machine's operation. Water enters at the upper level, fills the cavities between consecutive blades and descends along the helical surface under the action of gravity, converting potential energy into work on the rotor. The resulting mechanical energy is transferred to a generator coupled to the shaft. The magnitude of the generated power depends on the available flow rate and on the head difference between the upstream and downstream water levels, and the fill level of the cavities is the variable that governs the effective efficiency [15, 17].

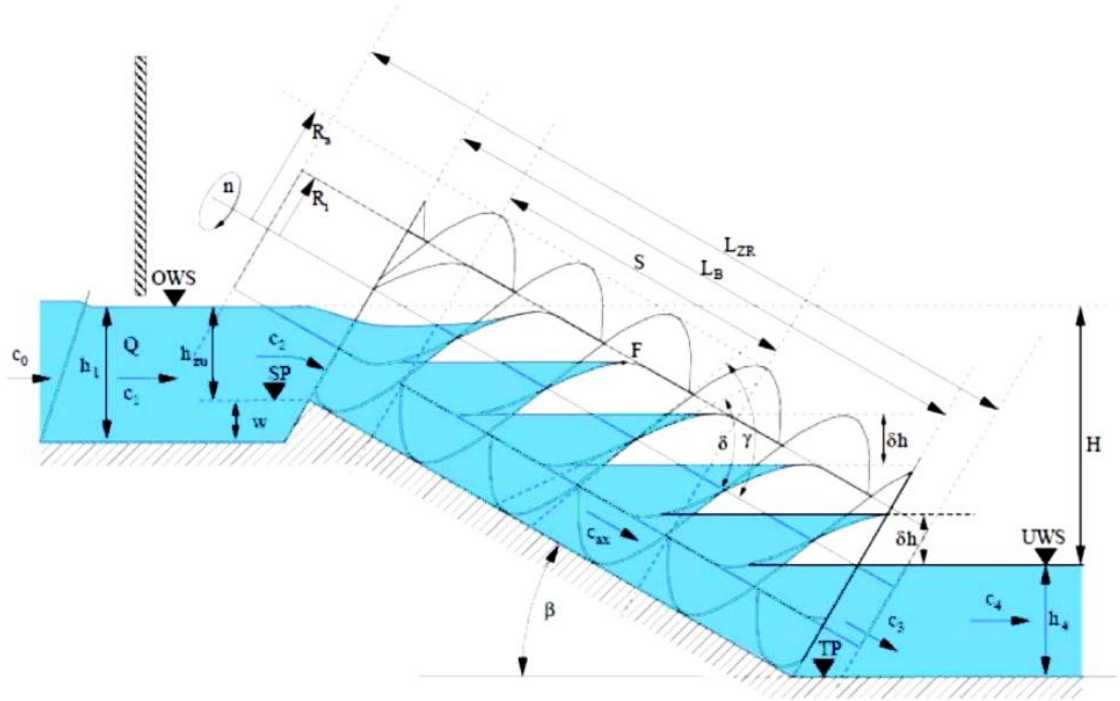


Figure 1. Operating principle of an Archimedes screw turbine: upstream (OWS) and downstream (UWS) water levels, net head, inclination angle and helical-channel nomenclature. Schematic adapted from the standard representation in the hydraulic-screw literature [15, 17].

The object of study is a bench-scale prototype, whose three-dimensional model is shown in Figure 2: a short screw housed in a semicircular channel, mounted on a frame with pillow-block bearings and a transmission shaft. The scale of the device is relevant to everything that follows and, for that reason, is not taken from a statement in the text but from the axis annotations that appear in the study's own figures: the computational domain measures $D \leq 0{,}242$ m

in height and $L \approx 0{,}437$ m in length. The screw diameter is therefore bounded by 0.242 m. At the declared rotational speed, $N = 160$ rev min^{-1}, equivalent to $\omega = 16{,}76$ rad s^{-1}, the peripheral tip speed is $U_{\text{tip}} = \omega R = 2{,}03$ m s^{-1}.

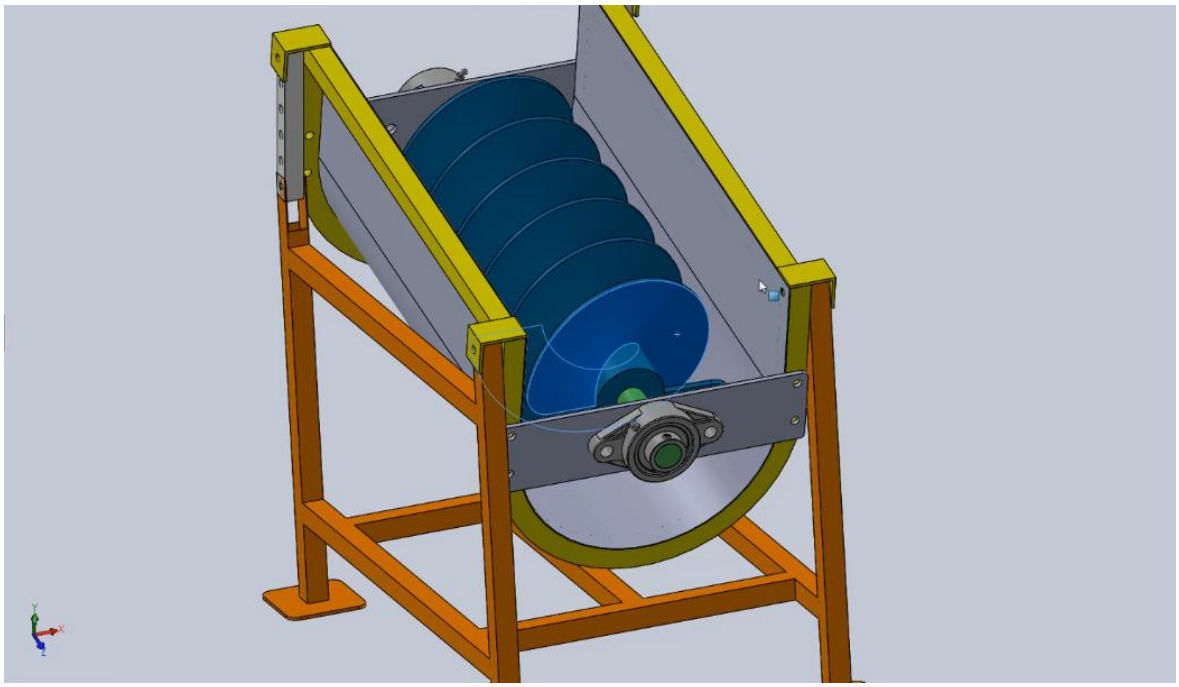


Figure 2. Three-dimensional model of the prototype: screw, channel, frame and transmission system. Screenshot from the computer-aided design environment used by the authors, cropped to remove interface elements.

2.3 Three-dimensional CFD model

The computational domain reproduces a segment of the helical channel with the screw housed inside it, in a closed prismatic volume. The rotor zone is solved in a rotating reference frame attached to the screw, which allows a flow that is not steady in the fixed frame to be treated as steady. The relation between the absolute velocity and the velocity relative to the rotating frame is the one in Eq. (3):

$$w = u - \Omega \times r \tag{3}$$

where u is the absolute velocity, w the velocity relative to the rotating frame, Ω the angular velocity vector and r the position vector with respect to the rotation axis.

2.3.1 Governing equations

Water is treated as an incompressible, isothermal, Newtonian fluid. Under these assumptions mass conservation reduces to the zero-divergence condition, Eq. (4):

$$\nabla \cdot u = 0 \tag{4}$$

and momentum conservation in the rotating frame, with constant angular velocity, takes the form of Eq. (5):

$$\rho\left[\frac{\partial w}{\partial t} + (w \cdot \nabla)w\right] = -\nabla p + \nabla \cdot \tau + \rho g - 2\rho(\Omega \times w) - \rho\Omega \times (\Omega \times r) \tag{5}$$

where the dependent variable is w, the velocity relative to the rotating frame defined in Eq. (3); p is the pressure, τ the viscous stress tensor, ρ the density and g the acceleration of gravity. The last two terms on the right-hand side are, respectively, the Coriolis acceleration and the centrifugal acceleration, both written in the same variable. The incompressibility condition of Eq. (4) is likewise satisfied for w, because the field $\Omega \times r$ is solenoidal. The term associated with the time variation of the angular velocity does not appear because the rotational regime is assumed constant.

No energy equation is solved. The problem is isothermal and the fluid incompressible, so the temperature field is decoupled from the velocity and pressure fields and carries no information about the machine's operation. The only energy balance with physical content in this problem is the hydraulic one in Eqs. (1) and (2), which relates head, flow rate, torque and efficiency.

Turbulence closure is carried out with a two-equation k-ε type model. The turbulence intensity imposed at the inlet is 1.5% and the turbulent length scale is 10 mm.

The flow regime justifies that closure, and it is worth establishing it with numbers rather than assuming it. With the Reynolds number defined by Eq. (6):

$$\mathrm{Re} = \frac{\rho V D_{\mathrm{h}}}{\mu} \tag{6}$$

and evaluated with the properties of water at 20 °C, a characteristic velocity of the order of 2 to 4 m s^{-1} taken from the calculated field, and a hydraulic diameter between 0.05 m and the height of the domain, gives $\mathrm{Re} \approx 1 \times 10^5 - 1 \times 10^6$. The flow is fully turbulent throughout that range, and would remain so in a considerably smaller channel. The screw turbine is a machine with a low rotational speed, but that does not place it in the viscous regime: modelling its internal flow without a turbulence closure would not be justified.

2.3.2 Frozen-rotor approximation

The coupling between the rotating zone and the rest of the domain is handled with the frozen-rotor approximation, which keeps the relative position between the two zones fixed and solves the problem in steady state. It is used here because it is a computationally economical steady-state approximation, not because its fidelity is established for this system. The higher-fidelity alternatives — mixing plane and, above all, sliding mesh, which allows the physical rotation of the mesh — resolve the interaction between zones in a progressively more complete way at the cost of longer computation time, and neither has been executed in this work. The 59% discrepancy documented in Section 3.2 is precisely a reason not to attribute fidelity to the approximation used without that comparison.

2.3.3 Boundary conditions and status of the computational record

The boundary conditions documented for the study are an imposed velocity at the inlet section and an imposed total pressure at the outlet, with the channel walls and the screw surface treated as solid boundaries and the rotor zone defined as a rotating region. The reported solution corresponds to iteration 140.

What follows is a statement of scope, not a minor limitation: much of the computational record on which a claim of numerical fidelity would depend could not be recovered. Table 1 summarizes it element by element, distinguishing what is documented from what is not. Declaring these gaps has been preferred over reconstructing them, because a numerical verification that was not run cannot be reported.

Element	Status in the available record	Consequence for what can be claimed
Mesh convergence study	Not recoverable. The study documents a single global mesh, with no systematic refinements or cell counts.	The results are interpreted as one numerical realization and not as mesh-independent predictions. The terms «mesh-independent» and «accurate» are not used.
Grid convergence index (GCI)	Not computable: it requires at least three systematically refined meshes [4].	The discretization uncertainty of the reported field is not bounded.
Residual history and mass balance	Not recoverable. Only the iteration number reached is recorded.	Iterative convergence is not documented. That the solver produced a result is not evidence of convergence.
Wall resolution (y^+)	Not recoverable.	The compatibility between the turbulence model and the wall treatment is not verified. Sensitivity to the turbulence model remains unresolved.
Free-surface model	The domain is a closed volume, completely flooded, with a single phase.	The model does not resolve the water-air interface. The physics of partial filling of the cavities, which governs the actual performance of the machine [15], is not represented.
Shaft torque	Not reported.	The mechanical closure $P_{\mathrm{s}} = T\omega$ cannot be checked independently.

Table 1. Status of the recoverable computational record and its effect on admissible claims.

One point of that table is underlined because it conditions the interpretation of the entire study. The domain is a closed, fully flooded volume, solved with a single phase. A real screw turbine operates with partially filled cavities and a free surface in each of them; the fill level is, in fact, the variable that governs its efficiency [15]. The model used here does not capture that physics. A multiphase treatment with interface tracking is the necessary extension, and it remains as future work.

2.4 Gated verification protocol

The checks above are not a checklist: they have an order, and the order matters, because each one conditions the meaning of the next. Comparing two models cell by cell before knowing whether their units are consistent produces figures that mean nothing. They are therefore organized as a four-gate decision sequence on model fidelity, collected in Table 2, which is how this work connects with operations research: not as a weighting of criteria, but as a resource-escalation policy for verification.

Gate	Question	Pass criterion	If it fails
G1	Dimensional consistency	The operating point closes $P_h = \rho g Q H$ and the velocity scales are compatible with the geometry and the rotational regime.	Interpretation of ABSOLUTE MAGNITUDES stops. Scale-invariant comparisons can continue, but only for pairs in which both values can be shown to share the same scale factor and the same physical provenance.
G2	Numerical and conservation consistency	Documented iterative convergence, closed mass balance and a mesh convergence study with bounded discretization uncertainty [4].	Report the result as a single numerical realization, without attributing mesh independence or accuracy to it.
G3	Discrepancy tolerance between models	Each cell-by-cell comparison lies within the declared tolerance, here 15 %. That figure is the design study's own claim being checked, not a general accuracy criterion: lying within it does not validate the model.	Locate the failing cell, do not average it with those that pass, and treat it as a hypothesis about the responsible mechanism.
G4	Escalation decision	—	Depending on the gate that fails: G1 requires revising the 1D design; G2 requires redoing the numerical verification; G3 requires higher-fidelity CFD —transient, with sliding mesh and free surface— and, ultimately, experimental measurement.

Table 2. Gated verification protocol. There are no weights or aggregation: the sequence is purely ordinal, and each gate determines which claims remain available from it onward.

The G1 proviso deserves to be made precise, because whether this work can do anything after the first gate fails depends on it. A relative error is invariant under a change of scale: if the two values of a pair are multiplied by the same positive constant $c > 0$, the ratio does not change, per Eq. (7):

$$\frac{|cX_{\mathrm{CFD}} - cX_{1\mathrm{D}}|}{|cX_{1\mathrm{D}}|} = \frac{|X_{\mathrm{CFD}} - X_{1\mathrm{D}}|}{|X_{1\mathrm{D}}|}, \quad c > 0 \tag{7}$$

The condition is exactly the one written in the statement and should not be assumed: the same factor c has to apply to BOTH values being compared. If the 1D design value and the CFD model value come from different scales, or from different calculations, the ratio ceases to be invariant and ceases to mean anything. That is why the provenance check comes before the comparison, and why Section 3.2 separates the comparisons whose provenance is established from those whose provenance is not.

This protocol is a resource-escalation policy for verification, not an optimization method. Its value lies in the order — dimensional consistency, numerical verification, discrepancy diagnosis, higher-fidelity model or experiment — not in

any supposed mathematical optimality, which is neither claimed nor demonstrated here. There are no weights, no aggregation and no objective function.

3. RESULTS AND VERIFICATION

3.1 Dimensional consistency audit (gate G1)

The published operating point states a hydraulic efficiency of 32%, a rotational speed of 160 rev min^{-1}, a flow rate with numerical value 1.45 and a power with numerical value 199.80. The units of the last two quantities are the object of this section, because as reported — 1.45 kg s^{-1} and 199.80 kW — the balance in Eq. (1) would require a head of 14,046 m, a magnitude with no correspondence to any hydraulic installation. The problem is not the hydraulic model: it is a scale factor in the report.

There are two readings that close the energy balance, and it is worth stating them before discarding either, because both are algebraically admissible:

Reading A: the flow rate is 1.45 m^3 s^{-1} and the power is 199.80 kW.

Reading B: the flow rate is 1.45 L s^{-1} and the power is 199.80 W.

Both lead to exactly the same head, 14.07 m, which identifies the problem as a factor of 1000 applied consistently, and not as an error in the hydraulic calculation. Choosing between them because one seems more plausible than the other would not be a verification. The choice is made here against geometric evidence taken from the study's own figures.

Velocity scale.

The colour bar of Figure 5b bounds the calculated velocity field below 12.79 m s^{-1}. The highest value in the comparison table is 416.35. Read in metres per second it would be 32.55 times the maximum of the field the study itself publishes, which is impossible. Read in centimetres per second it is 4.16 m s^{-1}, i.e. 2.05 times the tip speed at the periphery of the screw, an entirely normal magnitude in a helical channel. An independent check leads to the same conclusion: reaching 416.35 m s^{-1} while rotating at 160 rev min^{-1} would require a radius of 24.8 m, against the 0.121 m that the domain height allows at most. Centimetres per second is therefore declared as the unit of the velocity columns.

Flow-rate scale.

The same evidence resolves the choice between readings A and B. The channel's cross-section cannot exceed 0.0460 m^2, which is that of the circle whose diameter equals the domain height; any partial filling reduces it, and with it the mean velocity increases. With that bound, a flow rate of 1.45 m^3 s^{-1} would require a mean velocity of 31.5 m s^{-1}, 2.5 times the maximum of the calculated field. Reading A is excluded. A flow rate of 1.45 L s^{-1} gives 0.0315 m s^{-1}, compatible with the field. The flow-rate scale is resolved: litres per second.

Power scale: unresolved.

With the flow rate resolved, reading B would fix the hydraulic power at 199.80 W. That figure, however, does not withstand the same geometric check. The head available to the machine cannot exceed the length of the modelled segment, 0.437 m, and would only equal it in the limiting case of a vertical screw; Figure 2 shows an inclination far from that limit. Even taking that generous upper bound, the hydraulic power available with a flow rate of 1.45 L s^{-1} is 6.21 W. The declared power exceeds that bound by 32.2 times under reading B, and by more than thirty thousand under reading A. Neither reading is sustainable for this machine.

The conclusion of this gate must be stated without softening it. The dimensional audit identifies a factor-of-1000 ambiguity; the information available in the design report and its figures is consistent with the W and L s^{-1} interpretation for the flow rate, but does not independently establish the value of the power, which turns out to be incompatible with the device's geometric scale. The net head is not documented anywhere and the shaft torque is not reported, so neither the absolute power nor the efficiency can be verified. The input file of the original 1D design, or the geometric head

bound between the prototype's upstream and downstream water levels, is required to resolve it definitively. Until then the operating point is declared unverified, and no power figure from this work should be cited as a result.

A fourth inconsistency of the same kind remains open. The colour bar of Figure 5a places the entire pressure field between 101,268.60 and 101,390.95 Pa, i.e. an interval of 122.35 Pa around atmospheric pressure. The comparison table, in contrast, reports a static-pressure increase between inlet and outlet of 150.14 kPa, about 1,227 times that interval. A pressure jump of that magnitude cannot occur within a domain whose entire field spans 122.35 Pa. The two values therefore do not come from the same calculation, and the provenance of the table's pressure column cannot be established with the available record.

It is worth stressing, to avoid a mistaken reading of all of the above, that none of these scale corrections alters the relative errors of the VELOCITY rows in the next section. In those rows the two compared columns are affected by the same factor: the reading in cm s^{-1} holds equally for the 1D design and for the CFD, so the condition of Eq. (7) is satisfied and the 59.04% finding in the inlet tangential velocity remains exactly the same under either reading. For the two PRESSURE rows that condition cannot be taken as satisfied, and Section 3.2 treats them separately for that reason. Table 3 summarizes the audit magnitude by magnitude.

G1 is therefore not passed. What remains permitted after that failure is fixed by the rule in Section 2.4: absolute magnitudes are left outside interpretation, and relative comparisons remain available only for the pairs in which the same scale factor and the same provenance can be demonstrated. The next section applies that condition pair by pair, and not all of them satisfy it.

Quantity	Published value	Check applied	Status
Rotational speed	160 rev min^{-1}	16.76 rad s^{-1} by direct conversion; the reported value was 195.89 rad s^{-1}, which corresponds to 1 870 rev min^{-1}	Corrected
Unit of the velocities	m s^{-1}	the tabulated maximum would be 32.55 times the upper bound of the CFD field in Figure 5b	Corrected to cm s^{-1}
Flow rate	1.45 (disputed unit)	1.45 m^3 s^{-1} would require a mean velocity of 31.5 m s^{-1} in the maximum channel section	Resolved: L s^{-1}
Power	199.80 (disputed unit)	geometric bound on the available hydraulic power: 6.21 W	NOT RESOLVED
Net head	not declared	the energy balance would require 14.07 m; the geometry allows at most 0.437 m of elevation difference	NOT RESOLVED
Static pressure	84.10 → 241.64 kPa (1D); 92.05 → 242.19 kPa (CFD)	the pressure field in Figure 5a spans 122.35 Pa in total	NOT RESOLVED
Shaft torque	not reported	without torque, the mechanical closure of Eq. (2) cannot be checked; the shaft power that would be obtained is by definition 32 % of the hydraulic power, not an independent check	Not checkable

Table 3. Dimensional audit of the operating point. The contrast relies on the geometry and the field ranges documented in the study's own figures, not on external assumptions.

3.2 Audit of the published table and cross-verification (gate G3)

The study summarizes the agreement between the 1D design and the CFD model by stating that the difference between the two approaches «does not exceed 15%». That figure is the claim audited here, and it is worth saying from the outset what it is NOT: it is not a general CFD accuracy criterion, it does not come from any verification standard, and falling below it does not validate a model. It is the design study's own quantitative statement, and it is checked on its own terms.

The check is done by disaggregating: the relative error of each of the eight published comparisons — four variables at two stations — is computed taking the 1D design as the reference, per Eq. (8):

$$\varepsilon_{\mathrm{i}} = \frac{|X_{\mathrm{CFD,i}} - X_{\mathrm{1D,i}}|}{|X_{\mathrm{1D,i}}|} \times 100\ \% \tag{8}$$

The inlet radial-velocity cell is zero in both models by definition of the boundary condition, so its relative error is undefined and it is excluded from the computation; 7 comparisons with a non-zero reference remain, collected in Table 4.

Now, these seven comparisons are not all of the same nature, and treating them as if they were would be exactly the error this work exists to avoid. Two things must be separated:

(A) The arithmetic audit of the published table: checking that the ratios are correctly computed and that the 15% claim holds on the figures as published. It covers the seven comparisons.

(B) The physically traceable cross-verification: reading those ratios as an actual contrast between two models of the same flow. It only admits the pairs that satisfy the condition of Eq. (7), i.e. the same scale factor and the same provenance in both values.

The two pressure rows pass (A) and fail (B). Their ratios are correct, but as established in Section 3.1 their range is incompatible with the pressure field shown in Figure 5a: they cannot come from the reported calculation, and it is therefore not known what they are comparing. Table 4 marks this row by row.

Variable	Unit	Station	1D design	CFD (mean)	ε_i **(%)**	Interpretable as verification
Static pressure	kPa	Inlet	84.10	92.05	9.45	no — provenance not resolved
Static pressure	kPa	Output	241.64	242.19	0.23	no — provenance not resolved
Radial velocity	cm s^{-1}	Inlet	0.00	0.00	undefined (0/0)	yes
Radial velocity	cm s^{-1}	Output	298.24	332.20	11.39	yes
Tangential velocity	cm s^{-1}	Inlet	28.00	44.53	59.04	yes
Tangential velocity	cm s^{-1}	Output	361.31	335.02	7.28	yes
Relative velocity	cm s^{-1}	Inlet	243.00	275.75	13.48	yes
Relative velocity	cm s^{-1}	Output	363.36	416.35	14.58	yes

Table 4. Cell-by-cell relative error between the 1D design and the average CFD model. The last column distinguishes the arithmetic audit from the cross-verification: the pressure rows are arithmetically correct but not interpretable as a contrast between models until their provenance is resolved. The unit of the velocity columns is the one established in Section 3.1.

Result (A): the study's claim holds arithmetically.

Six of the seven comparisons with a non-zero reference fall within 15%. The exception is the tangential velocity at the screw inlet: 28.00 cm s^{-1} in the 1D design against 44.53 cm s^{-1} in the CFD average, a relative error of 59.04%, nearly four times the bound and the highest in the entire table.

Result (B): of what is actually traceable, four of five.

Discounting the two pressure rows, five velocity comparisons remain whose provenance is established and in which the same scale factor affects both columns. Of these, four fall within 15% — with a maximum of 14.58% — and one falls outside it, the one already cited, at 59.04%. This is the figure that can be read as internal consistency between the two models, and it is more modest than the first: the demonstrable agreement covers four velocity pairs, not six comparisons of every kind.

The mean absolute percentage error over the seven comparisons is 16.49%. This figure is reported as an aggregate descriptor and nothing more. It averages pressures with radial, tangential and relative velocities, quantities of different dimension and physical meaning, and it further mixes traceable rows with rows that are not; it has no mechanistic interpretation and should not be used as a model-validity statistic. The result with scientific content is the vector of individual discrepancies in Table 4, and in particular its maximum component: a single summary figure would have concealed precisely the cell that orients the subsequent work.

That discrepancy is not a detail. The study's own theoretical framework identifies the tangential velocity component as the one that determines the torque delivered to the shaft, so a disagreement of this magnitude at the inlet directly

affects the mechanical quantity on which torque production depends. Its origin, however, cannot be established with the available information. The most economical explanation is a reference-frame difference between the two compared columns — absolute velocity versus velocity relative to the frame, linked by Eq. (3) — or a difference in the measurement station, given that the tangential component varies rapidly in the inlet zone. Attributing it to the frozen-rotor approximation would be plausible, because that approximation is least faithful precisely where the flow has not yet adapted to the rotating frame, but establishing it would require a sliding-mesh comparison that this work does not carry out. The discrepancy is reported as bounded and its cause is left open.

3.3 CFD fields and interpretation

Figures 3 to 5 present the calculated field. Figure 3 shows the contour on the surface of the screw and the channel, with the axis annotations that fix the geometric scale used in Section 3.1.

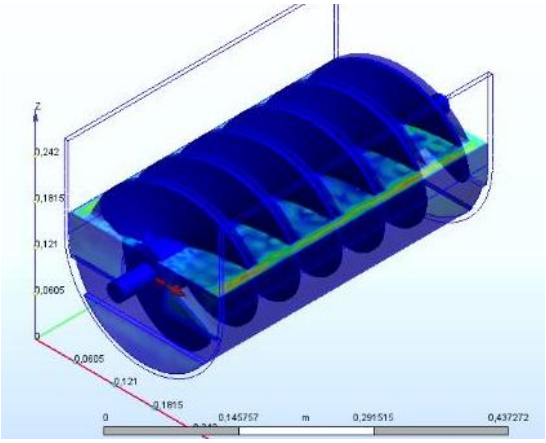
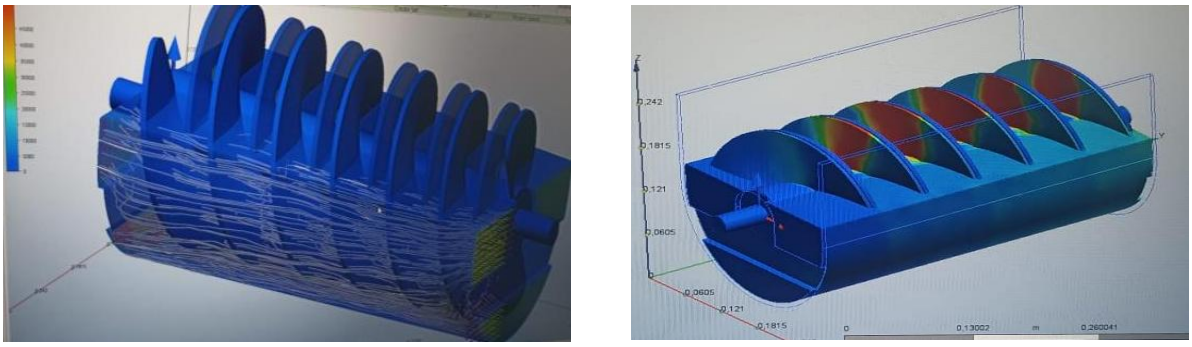


Figure 3. Calculated field on the surface of the screw and the channel. The axis annotations fix the domain scale: 0.242 m in height and 0.437 m in length.

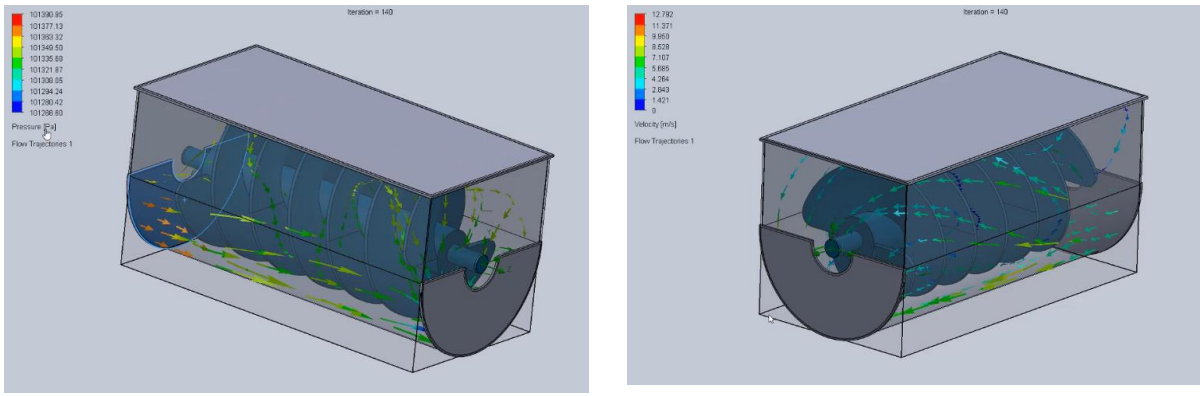
Qualitatively, the field is what would be expected from a confined helical channel: the flow adapts to the rotation along the first stretch, develops the helical pattern in the central zone and accelerates at the periphery of the blade, where the maximum velocity values are located, as shown by the pathlines in Figure 4. Nothing observed contradicts the expected behaviour. But it is worth being explicit about the scope of this reading: without a residual history, a mass balance or a mesh-convergence study, the qualitative coherence of the field cannot be taken as evidence of numerical accuracy. A field can look plausible and still be poorly resolved.



(a) (b)

Figure 4. (a) Flow pathlines along the helical channel. (b) Contour in the axial direction, with the domain scale annotated. Both images are screenshots from the simulation environment used by the authors; they are reproduced as they appear in the available record, cropped of interface elements.

To the above is added a model limitation that conditions the physical interpretation of these figures, and that is visible in them: the domain is a closed, fully flooded volume and the calculation is single-phase. The real machine operates with partially filled cavities, and the fill level is the variable that governs its efficiency [15]. The fields in Figures 3 to 5 therefore describe the flow around a submerged screw, not that of a screw turbine in gravitational operation. Figure 5 presents the two fields whose colour bars are legible — pressure and velocity magnitude — and whose ranges support the audit in Section 3.1.



(a) (b)

Figure 5. Calculated fields with their ranges: (a) pressure, between 101,268.60 and 101,390.95 Pa; (b) velocity magnitude, between 0 and 12.79 m s^{-1}. The label indicates that the reported solution corresponds to iteration 140.

4. DISCUSSION AND LIMITATIONS

The main result of this work is negative, and it is the one that carries the most information. Of the four gates in the Section 2.4 protocol, the first — dimensional consistency — is not passed: the published operating point does not close the hydraulic energy balance under either of the two algebraically admissible scale readings, and the declared power exceeds by more than an order of magnitude the bound imposed by the device's own geometry. The second gate is not passed either, for lack of record: there is no mesh-convergence study, no residual history, no mass balance. The third is passed in six of seven arithmetic comparisons; on what is physically traceable, agreement is reduced to four of five velocity comparisons, and the remaining one fails, at 59.04%.

Table 5 presents the outcome of the four gates, and the order in which they are applied explains why this matters. The failure of G1 does not void everything that follows, but it precisely bounds what survives: absolute magnitudes cease to be interpretable, while relative ratios remain so for the pairs in which the same scale factor affects both values, by Eq. (7). That condition is satisfied in the velocity rows and cannot be taken as satisfied in the pressure rows, whose provenance remained unresolved. The transferable lesson is that dimensional verification must precede the comparison between models and determine which part of it is admissible, rather than accompanying it as a courtesy check. Rigorously separating divergence attributable to geometric discrepancies from a lack of information or mesh resolution avoids the methodological collapse between conflict and ignorance, in line with the typed evaluation models of Leyva Vázquez [14]. The systematic comparison and selection among simulation representations of different computational cost and fidelity follows the multicriteria evaluation principles for choosing algorithmic models formulated by Leyva Vázquez et al. [13].

It is also worth stating what this protocol is and is not. It is a resource-escalation policy for verification: a decision sequence on model fidelity that orders when it is worth spending on a more expensive calculation or on an experiment. It is not an optimization method, it carries no weights, it aggregates no criteria, and the sequence is not claimed to be mathematically optimal. Its value lies in the order and in each gate declaring which claims remain available after it.

Gate	Result in this study	Escalation implied
G1 — dimensional consistency	NOT PASSED. Velocity and flow-rate scales resolved; power and head not. Reading of absolute magnitudes stops; relative comparisons remain admissible where the same scale factor and the same provenance are shown.	Recover the input file of the 1D design and the geometric head of the prototype.
G2 — numerical consistency	NOT PASSED for lack of records: no mesh convergence, no residuals, no mass balance.	Redo the numerical verification with at least three systematic meshes and a convergence index [4].
G3 — discrepancy audit	Arithmetic: 6 of 7 within 15 %. Physically traceable: 4 of 5 velocities; the inlet tangential velocity fails at 59.04 %. The 2 pressure rows are excluded.	Higher-fidelity CFD: transient, with sliding mesh and a free-surface model.
G4 — escalation decision	The three previous gates point in the same direction.	Experimental measurement of torque, flow rate, head and efficiency on the prototype, which is the only thing that can validate the model.

Table 5. Result of the verification protocol applied to this study.

The limitations bounding this work are consequently extensive, and listing them is not a formality. The CFD model is steady, single-phase and single-mesh, solved under a frozen-rotor approximation whose fidelity for this system is not established. It does not resolve the free surface and therefore does not represent the partial filling of the cavities, which is the physical mechanism that governs the machine's efficiency. No wall resolution is available, and consequently neither is verification of the compatibility between the turbulence model and its wall treatment, nor a sensitivity analysis to the turbulence model. Shaft torque is not reported, so the mechanical closure between hydraulic power and useful power cannot be checked independently. And there is no experimental measurement of any quantity.

From this follows what this work cannot claim, which it is worth declaring as explicitly as the results. It cannot claim that the CFD model is accurate, or that it is mesh-independent, or that it is validated. It cannot sustain any power or efficiency figure as a result of the study. And it cannot attribute the inlet tangential-velocity discrepancy to any specific cause. And it cannot read the two pressure rows as verification between models while their provenance remains unestablished. What it can claim is that the published table is arithmetically correct in six of its seven comparisons; that of the five velocity comparisons, which are the traceable ones, four agree within 15% under a now-explicit unit scale and one disagrees severely; and that the published operating point is not dimensionally consistent with the machine it describes.

5. CONCLUSIONS

The dimensional audit of the operating point identifies scale inconsistencies that invalidate the published absolute magnitudes. The rotational speed was reported with an erroneous conversion to radians per second; the velocity columns had been labelled m s^{-1} when their values are consistent with cm s^{-1}, i.e. on a scale 100 times larger than the one compatible with the calculated field; and the flow-rate—power pair, affected by a factor-of-1000 ambiguity. The velocity scale and the flow-rate scale are resolved against the geometry documented in the study's figures: centimetres per second and litres per second, respectively. The power scale is not resolved: the declared figure exceeds by 32.2 times the bound imposed by the device's geometry, and determining it requires the input file of the 1D design or the prototype's geometric head bound. The net head is not documented and the shaft torque is not reported, so neither the absolute power nor the device's efficiency can be verified with the existing information.

On the comparison table, two claims that do not carry the same weight must be distinguished. The arithmetic audit of the published table places 6 of its 7 non-zero-reference comparisons within 15%. But only the velocity comparisons can be interpreted physically: the two pressure rows are excluded because their range is incompatible with the pressure field shown by the study's own figure, and their provenance cannot be established. Of the five velocity comparisons, four fall within 15%, with a maximum of 14.58%, and the tangential velocity at the screw inlet is the exception, at 59.04%. Its cause remains unresolved: the more economical hypotheses — a difference in reference frame or in

measurement station — cannot be discriminated with the available information, and attributing it to the frozen-rotor approximation would require a sliding-mesh comparison that has not been carried out.

Those four velocity agreements support limited internal consistency between two models of the same design, and nothing more. They are not physical validation. The two models share hypotheses, boundary conditions and author, so their agreement is a necessary condition of correctness and not evidence of it. The absence of a mesh-convergence study and of experimental measurement further prevents attributing predictive capability to the results: they are a single numerical realization. And the pressure comparisons cannot be read in any physical sense until it is documented where they came from.

The next step is determined by the gate that fails first. In order: recover the input file of the 1D design to close the scale of the operating point; run a mesh verification with at least three systematic refinements and a convergence index [4]; replace the single-phase steady model with a transient sliding-mesh calculation with free-surface tracking, capable of representing the partial filling of the cavities [15]; and measure torque, flow rate, head and efficiency on the prototype, which is the only one of the four actions that can turn this verification into validation.

The transferable part of this work is not the design of this turbine, but the gated protocol with which it was examined. It orders the fidelity checks so that each conditions the meaning of the next, makes explicit which claims remain available after each failure, and turns the decision to escalate toward a more expensive model — or toward the laboratory — into a consequence of the evidence rather than of resource availability. It is applicable to any study that contrasts a design model with a detailed simulation. The same escalation logic applies in any case where a cheaper, coarser check is run before a more expensive one — dimensional consistency before mesh-independent CFD, order-of-magnitude bounds before a full experiment — which is a reproducibility concern in engineering broader than this particular turbine.

ACKNOWLEDGEMENTS

Data availability: the dimensional audit and the calculation of the relative errors in Table 4 are reproduced in full from the values published in this article and from the geometric scales annotated in Figures 3 to 5. The original computational project is not available.

RECEIVED: MAY, 2026;
REVISED: OCTOBER, 2026.

REFERENCES

[1]. M. ALONSO-MARTINEZ, J. L. S. SIERRA, J. J. D. C. DÍAZ and J. E. MARTINEZ-MARTINEZ (2020): A new methodology to design sustainable archimedean screw turbines as green energy generators. **International Journal of Environmental Research and Public Health**, 17, 9236. https://doi.org/10.3390/ijerph17249236

[2]. J. BETANCOUR, L. VELÁSQUEZ, L. Y. JARAMILLO, E. CHICA and A. RUBIO-CLEMENTE (2021): Application of a central composite face-centered design in the optimization of an archimedean hydrokinetic turbine. **Renewable Energy and Power Quality Journal**, 19, 308-313. https://doi.org/10.24084/repqj19.308

[3]. S. BORAH, B. CHOWDHURY, S. GOGOI and Z. ASKARY (2015): A theoretical study of design parameters of an Archimedean screw turbine. National Institute of Technology, Silchar, India.

[4]. I. B. CELIK, U. GHIA, P. J. ROACHE, C. J. FREITAS, H. COLEMAN and P. E. RAAD (2008): Procedure for estimation and reporting of uncertainty due to discretization in CFD applications. **Journal of Fluids Engineering**, 130, 078001. https://doi.org/10.1115/1.2960953

[5]. A. DRAGOMIRESCU (2021): Design considerations for an Archimedean screw hydro turbine. **IOP Conference Series: Earth and Environmental Science**, 664, 012034. https://doi.org/10.1088/1755-1315/664/1/012034

[6]. K. ENOKIZONO, Y. SHII and T. TABATA (2018): Flow analysis around Archimedean screw hydraulic turbine using OpenFOAM. **Proceedings of the Conference of the Kyushu Branch of the JSME**, 2018.71, A25. https://doi.org/10.1299/jsmekyushu.2018.71.a25

[7]. E. ERINOFIARDI, R. KOIRALA, N. SHIWAKOTI and A. DATE (2022): Sustainable power generation using Archimedean screw turbine: influence of blade number on flow and performance. **Sustainability**, 14, 15948. https://doi.org/10.3390/su142315948

[8]. E. FIARDI (2014): Preliminary design of Archimedean screw turbine prototype for remote area power supply. **Journal of Ocean, Mechanical and Aerospace Science and Engineering**, 5, 30-35.

[9]. A. KHAN, A. KHATTAK, A. ULASYAR, K. IMRAN and M. A. MUNIR (2019): Investigation of Archimedean screw turbine for optimal power output by varying number of blades. **1st International Conference on Electrical, Communication and Computer Engineering (ICECCE)**, Swat, Pakistan. https://doi.org/10.1109/ICECCE47252.2019.8940654

[10]. U. KUMAR, P. SINGH and A. C. TIWARI (2016): Suitability of Archimedes screws for micro hydro power generation in India. **International Journal of Thermal Technologies**, 6, 273-278.

[11]. A. LASHOFER, F. KALTENBERGER and B. PELIKAN (2011): Wie gut bewährt sich die Wasserkraftschnecke in der Praxis? [Does the Archimedean screw turbine stand the test?]. **Wasserwirtschaft**, 101, 7-8.

[12]. A. LASHOFER, W. HAWLE and B. PELIKAN (2013): Efficiency improvements of the Archimedean screw turbine. **WasserWirtschaft**, 103, 7-8. https://doi.org/10.1365/s35147-013-0647-0

[13]. M. Y. LEYVA VÁZQUEZ, L. A. BRIONES PEÑAFIEL, S. X. SÁNCHEZ MUÑOZ and M. A. QUIROZ MARTÍNEZ (2021): A Framework for Selecting Machine Learning Models Using TOPSIS. **Advances in Intelligent Systems and Computing**, 1213, 119-126. https://doi.org/10.1007/978-3-030-51328-3_18

[14]. M. Y. LEYVA VÁZQUEZ (2026): Typed Evaluation Models and the Collapse Between Conflict and Ignorance: A Case Study on Jev. **Neutrosophic Computing and Machine Learning**, 45. https://fs.unm.edu/NCML_2/index.php/NCML/article/view/186

[15]. W. D. LUBITZ, M. LYONS and S. SIMMONS (2014): Performance model of Archimedes screw hydro turbines with variable fill level. **Journal of Hydraulic Engineering**, 140, 10. https://doi.org/10.1061/(ASCE)HY.1943-7900.0000922

[16]. B. MAYRHOFER, A. STERGIOPOULOU, B. PELIKAN and E. KALKANI (2014): Towards an innovative radial flow impulse turbine and a new horizontal Archimedean hydropower screw. **Journal of Energy and Power Sources**, 1, 2.

[17]. G. MÜLLER and J. SENIOR (2009): Simplified theory of Archimedean screws. **Journal of Hydraulic Research**, 47, 666-669. https://doi.org/10.3826/jhr.2009.3475

[18]. A. SALAM, J. M. ISSAC and B. MARKOSE (2018): Numerical study of Archimedean screw turbine. **International Research Journal of Engineering and Technology**, 5, 4.

[19]. K. SHAHVERDI (2021): Modeling for prediction of design parameters for micro-hydro Archimedean screw turbines. **Sustainable Energy Technologies and Assessments**, 47, 101554. https://doi.org/10.1016/j.seta.2021.101554

[20]. A. STERGIOPOULOU, V. STERGIOPOULOS and E. KALKANI (2013): Contributions to the study of hydrodynamic behaviour of innovative Archimedean screw turbines recovering the hydropotential of watercourses and of coastal currents. **Proceedings of the 13th International Conference on Environmental Science and Technology**, Athens, Greece.

[21]. A. STERGIOPOULOU and E. KALKANI (2015): Towards a first CFD study of modern horizontal axis Archimedean water current turbines. **International Research Journal of Engineering and Technology**, 2, 3.

[22]. M. ZAMANI, R. SHAFAGHAT and B. A. KHARKESHI (2023): Experimental investigation on the effect of flow rate and load on the hydrodynamic behavior and performance of an Archimedes screw turbine. **International Journal of Engineering, Transactions A: Basics**, 36, 726-736. https://doi.org/10.5829/ije.2023.36.04a.12